

1                                    **The missing role of gray matter in studying brain controllability**

2    Hamidreza Jamalabadi<sup>1\*</sup>, Agnieszka Zuberer<sup>1,2,3,7\*</sup>, Vinod Jangir Kumar<sup>6</sup>, Meng Li<sup>6</sup>, Sarah Alizadeh<sup>1</sup>, Ali  
3                                    Amani Moradi<sup>8</sup>, Christian Gaser<sup>7</sup>, Michael Esterman<sup>2,3,9,10</sup>, Martin Walter<sup>1,4,5,6,7</sup>

4    <sup>1</sup> Department of Psychiatry and Psychotherapy, University of Tübingen, Tübingen, Germany

5    <sup>2</sup> Boston University School of Medicine, Department of Psychiatry, Boston, USA

6    <sup>3</sup> Boston Attention and Learning Laboratory, VA Boston Healthcare System, Boston, USA

7    <sup>4</sup> Clinical Affective Neuroimaging Laboratory, Magdeburg, Germany

8    <sup>5</sup> Leibniz Institute for Neurobiology, Magdeburg, Germany

9    <sup>6</sup> Max Planck Institute for biological cybernetics, Tübingen, Germany

10   <sup>7</sup> Department of Psychiatry and Psychotherapy, Jena University Hospital, Jena, Germany

11   <sup>8</sup> School of Engineering, RMIT university, Melbourne, Victoria, Australia

12   <sup>9</sup> Neuroimaging Research for Veterans Center (NeRVE), Veterans Administration, Boston Healthcare System, Boston, USA

13   <sup>10</sup> National Center for PTSD, VA Boston Healthcare System, USA

14   \* equal contribution

15   **Corresponding Authors:** Hamidreza Jamalabadi (hamidreza.jamalabadi@uni-tuebingen.de), Department of Psychiatry and  
16   Psychotherapy, Division for Translational Psychiatry, University of Tübingen, Calwerstr. 14, 72076; Agnieszka Zuberer  
17   (azuberer@bu.edu), National center for PTSD, VA Boston Healthcare System, USA

18   **1 Abstract**

19   Brain controllability properties are normally derived from the white matter fiber tracts in which the  
20   neural substrate of the actual energy consumption, namely the gray matter, has been widely ignored.  
21   Here, we study the relationship between gray matter volume of regions across the whole cortex and  
22   their respective control property derived from the structural architecture of the white matter fiber  
23   tracts. The data suggests that the ability of white fiber tracts to exhibit control at specific nodes not

24 only depends on the connection strength of the structural connectome but additionally strongly  
25 depends on gray matter volume at the host nodes. Our data indicates that connectivity strength and  
26 gray matter volume interact with respect to the brain's control properties. Disentangling effects of the  
27 regional gray matter volume and connectivity strength, we found that frontal and sensory areas play  
28 crucial roles in controllability. Together these results suggest that structural and regional properties of  
29 the white matter and gray matter provide complementary information in studying the control  
30 properties of the intrinsic structural and functional architecture of the brain.

31 **Key words:** Network control theory, Gray matter, Brain controllability

32

## 33 **2 Introduction**

34 Network control theory, as recently applied to white matter (WM) fiber tracts in the human brain,  
35 provides a novel mechanistic framework to describe the ease of switching between different  
36 dynamical functional brain states, and the regions that best drive these dynamics (Bassett & Sporns,  
37 2017; John D Medaglia, 2019; John Dominic Medaglia, Pasqualetti, Hamilton, Thompson-Schill, &  
38 Bassett, 2017). This approach has the potential to inform theories of dynamic cognitive processes,  
39 clinical neuroscience, neurodegeneration, and brain reserve. Specifically, there is evidence that these  
40 global brain state transitions are impaired in clinical populations (Braun et al., 2019; Jeganathan et al.,  
41 2018; Kenett, Beaty, & Medaglia, 2018) and that such impairments can be traced back to specific driver  
42 nodes (Jeganathan et al., 2018; Yoed N Kenett et al., 2018; Muldoon et al., 2016; Zoeller et al., 2019).  
43 However, this far, these control properties have been exclusively derived from WM fiber tracts without  
44 the consideration of gray matter (GM) properties. Given the importance of GM properties for cognitive  
45 functioning and brain health, and the established interrelationships between white and gray matter, it  
46 has been suggested that regional gray matter integrity may be a critical contributor and proxy for  
47 network and node controllability (John Dominic Medaglia et al., 2017; J. D. Medaglia, Zurn, Sinnott-  
48 Armstrong, & Bassett, 2017).

49 Several lines of research suggest that GM may be essential to understanding brain controllability. First,  
50 GM is a proxy for the quantity of neurons and synaptic densities in a particular region (Lüders,  
51 Steinmetz, & Jäncke, 2002), and metabolic energy expenditure is primarily realized through the gray  
52 matter cell bodies that scaffold white matter tracts (Zhu et al., 2012). In neurodegenerative disorders,  
53 region specific lesions of GM only partially agrees with corresponding lesions in WM in some  
54 neurodegenerative disorders (Agosta et al., 2011; Bodini et al., 2009; Douaud et al., 2007; Raine, Lencz,  
55 Bihrlé, LaCasse, & Colletti, 2000; Villain et al., 2008), suggesting that GM reserve and WM may provide  
56 independent additional information with respect to controllability properties of the structural  
57 connectome. Taken together, these studies motivated the hypothesis that the controllability  
58 properties suggested by the WM should be partially related to or even predicted by GM integrity.  
59 Critically, it has been argued that including GM metrics in control theory will extend traditional  
60 volumetrics into network neuroscience (John Dominic Medaglia et al., 2017). Nevertheless, to our  
61 knowledge the nature of the interdependency between controllability properties and GM properties  
62 has not been addressed empirically.

63 To tackle this issue, we used two independent data sets to investigate whether, and if so, how control  
64 properties extracted from the structural connectome relate to properties of the gray matter, i.e. GM  
65 volume which engenders other GM metrics e.g. surface and thickness (Kong et al., 2015; Winkler et al.,  
66 2010). Since previous studies have shown that brain controllability can be largely explained by the  
67 connectivity strength of the structural connectome, we also considered whether GM volume could  
68 explain additional variance in controllability not accounted for by white matter connectivity. Initially,  
69 we investigated how WM and GM factors affect brain controllability on a whole brain level. In a further  
70 step, we identified the brain regions for which controllability was most sensitive to GM and/or WM  
71 properties. We discuss our findings with respect to their potential relevance to cognitive and clinical  
72 neuroscience.

### 73 **3 Methods and Materials**

## 74 **3.1 Data acquisition**

75 The structural and diffusion datasets are from 65 healthy subjects with the age range of 22 to 36 (28  
76 M, mean age 29.2) which were taken from the Human Connectome Project (HCP, Principal  
77 Investigators: David Van Essen and Kamil Ugurbil; 1U54MH091657; Van Essen et al., 2012). While HCP  
78 offers more than 1100 subjects, the data in the present study is limited by the resources necessary for  
79 preprocessing. We have tried to lift the potential bias by including an independent dataset (see  
80 replication study).

### 81 **3.1.1 MRI Data Specification**

82 Structural images were acquired with the following specification: T1w MPAGE, TR 2400 ms, TE 2.14  
83 ms, TI 1000 ms, flip angle 8 degrees, Field of View (FOV) 224x224, 256 slices, voxel size 0.7 mm  
84 isotropic, Bandwidth 210 Hz/Px, IPAT 2, acquisition time 7:40 min.

85 Diffusion weighted imaging (DWI) data were acquired by using a Spin-echo EPI sequence with TR 5520  
86 ms, TE 89.5 ms, flip angle 78 degrees, voxel size, 1.25 mm isotropic, 111 slices, multiband factor, 3,  
87 echo spacing, 0.78 ms, b-values 1000, 2000, and 3000 s/mm<sup>2</sup>. For details, see (Glasser et al., 2013; Van  
88 Essen et al., 2012).

### 89 **3.1.2 AAL mask definitions and native space transformation**

90 The 3-D anatomy atlas of the AAL2 was acquired from the neurofunctional imaging group  
91 (<http://www.gin.cnrs.fr/en/tools/aal-aal2/>) (Tzourio-Mazoyer et al., 2002). It contains 120 regions,  
92 which include subcortical structures i.e. thalamus, caudate, putamen, pallidum, etc. However, it misses  
93 the brainstem. The 12-parameter affine transformation (Jenkinson, Bannister, Brady, & Smith, 2002;  
94 Jenkinson & Smith, 2001) was computed for each volunteer's T1 and non-diffusion image and the MNI  
95 spaced standard brain. The resulted transformation matrix was applied to the left and right AAL brain  
96 regions to transform them into the native structural and diffusion space.

### 97 **3.1.3 Structural volume analysis**

98 The tissue type segmentation employed SPM12 unified segmentation approach. The process resulted  
99 in segmented gray, white, and cerebro-spinal fluid (CSF) volumes. In the next step, we determined the  
100 volume of the brain, gray matter, and under each AAL atlas region for all subjects. The skull extracted  
101 AC-PC aligned native spaced NIFTI structural scans were obtained from the Human Connectome  
102 database. In the next step, the tissue type segmentation was applied to delineate the gray matter  
103 within the brain using the SPM12 unified segmentation approach (Ashburner & Friston, 2005). This  
104 segmentation approach employs a generative model that combines non-linear registration, tissue  
105 classification, and bias correction.

#### 106 **3.1.4 Preprocessing and Diffusion-Fit**

107 The obtained HCP diffusion data were reconstructed using a SENSE1 algorithm (Sotiropoulos et al.  
108 2013). The DWI data was corrected for motion and distortion (Andersson et al. 2003; Andersson and  
109 Sotiropoulos 2015, 2016). Furthermore, pre-processing included unringing, denoising, and tensor  
110 analysis implemented in MRtrix (Tournier, Calamante, & Connelly, 2012).

111 The data were reconstructed using the multi-shell multi-tissue constrained spherical deconvolution  
112 (Jeurissen, Tournier, Dhollander, Connelly, & Sijbers, 2014). The resulted Orientation Distribution  
113 Function (ODF) was registered to the structural space. The initial tractogram was generated using  
114 mrtrix-tckgen, resulting in 100 million streamlines within each subject. In the next step, we applied  
115 spherical deconvolution informed filtering of tractograms (SIFT) to reduce the streamline count to 10  
116 million. In the final step, the number of streamlines was determined between AAL brain regions to  
117 produce a connectome. The analysis steps in more details are documented at the mrtrix docs i.e.  
118 ([https://mrtrix.readthedocs.io/en/latest/quantitative\\_structural\\_connectivity/structural\\_connectom](https://mrtrix.readthedocs.io/en/latest/quantitative_structural_connectivity/structural_connectome.html)  
119 [e.html](https://mrtrix.readthedocs.io/en/latest/quantitative_structural_connectivity/structural_connectome.html)).

#### 120 **3.2 Network control framework**

121 Controllability is one of the fundamental concepts in the control theory. The notion of controllability  
122 of a dynamical system was first introduced in (Kalman, 1963). State (output) controllability of a

123 dynamical system is defined as the possibility of driving states (outputs) of the system from an arbitrary  
124 initial condition to any desired values in finite time by applying appropriate control signals (Kailath,  
125 1980). The most famous classic method to ensure state controllability of a dynamical system defined  
126 by the noise-free linear discrete-time and time-invariant network model says that the system

$$127 \quad x(k + 1) = Ax(k) + Bu(k) \quad (1)$$

$$128 \quad y(k) = Cx(k) + Du(k) \quad (2)$$

129 is full state controllable if and only if the Kalman's controllability matrix  $[B, AB, \dots, A^{n-1}B]$  has full rank  
130 (Kailath, 1980). In the system represented in equations 1-2,  $\mathbf{x} \in \mathbb{R}^n$  and  $\mathbf{u} \in \mathbb{R}^p$  are state and input  
131 signals, respectively.  $A, B, C$  and  $D$  are matrices with appropriate dimensions where  $A$  and  $B$  are called  
132 state and input matrices, respectively. When applied in the context of brain controllability,  $\mathbf{x}$  describes  
133 the activity of brain regions.  $A$  is an adjacency matrix that represents the interactions between brain  
134 regions and its elements are often the strength of the white tracts connecting two areas (see section  
135 3.3 for details). The input matrix  $B$  identifies the control nodes in the brain which may be confined to  
136 one or more brain areas whose activities are denoted by the corresponding elements of  $\mathbf{x}$ . While the  
137 controllability matrix is a valuable metric to study the overall character of a system, it does not directly  
138 quantify potential ability of different nodes of the system to act as driver nodes. To achieve this, a  
139 common practice is to use  $Tr(W_k)$  which is the trace of the controllability Gramian  $W_k =$   
140  $\sum_{i=0}^{\infty} A^i B B^T (A^T)^i$  when the system is controlled from node  $k$ . Referred to as average controllability  
141 (AC), this metric is the most commonly used controllability measure in the neuroimaging literature (Gu  
142 et al., 2015; John D Medaglia, 2019) and is a measure of the average energy required for node  $k$  to  
143 steer the brain into all possible output states (see Tang & Bassett, 2018 a formal definition). In addition  
144 to AC that quantifies the ability of the nodes to drive the whole system into all potential target states,  
145 Modal Controllability (MC) is another commonly used metric which is a measure of the ability of the  
146 nodes to push the system toward difficult-to-reach states. Formally defined as  $\phi_k = \sum_j^N [1 -$   
147  $\xi_j^2(A)] v_{kj}^2$  MC is a scaled measure of difficulty of driving the system toward all  $N$  modes of  $A$  from  
148 node  $k$  (Pasqualetti, Zampieri, & Bullo, 2014).

### 149 3.3 Statistical analysis

150 Linear mixed effect (LME) regression (Baayen, Davidson, & Bates, 2008) allows to model the  
151 interrelation among multiple variables and has the ability to accommodate various experimental  
152 designs including repeated measurements, subject variability, and grouping structures in one unified  
153 implementation (Boisgontier & Cheval, 2016). In this paper, we model the interrelation between brain  
154 controllability (AC and MC), GM volume, and connectivity strength, for which we train multiple LMEs  
155 for different tasks. In these models, the elements  $A_{ij}$  of the structural connectivity matrix (i.e.  $A$  in  
156 equation 1) represent the number of streamlines between regions  $i$  and  $j$ . To ensure robustness, we  
157 keep only 10% of strongest connections using brain connectivity toolbox (Rubinov & Sporns, 2010).  
158 Within this scheme,  $i^{\text{th}}$  node degree is estimated by the sum of all elements of  $A$  in the  $i^{\text{th}}$  row. GM  
159 volume is estimated from the unified segmentation approach within SPM 12 (see section 3.1.3 for  
160 details). In particular, we include regional gray matter (rGM) and total intracranial volume (TIV) in the  
161 LMEs.

#### 162 3.3.1 LME formulation and statistical model comparison

163 To predict brain controllability metrics based on structural measures of the brain we built a linear  
164 mixed-effects (LME) regression (Baayen et al., 2008) using a step-wise approach retaining an effect  
165 only if there was a significant difference between the log-likelihood ratio of the two models, based on  
166 an ANOVA ( $p < 0.05$ ). Statistical analysis was performed using the lme4 package in R (Bates, Maechler,  
167 Bolker, & Walker, 2014). Specifically, we used two models. The first model is defined by controllability  
168 (AC/MC)  $\sim$  TIV+ Regions + Nodal degree \* rGM + (1|participants) where "\*" denotes the interaction  
169 where we are interested in quantifying the contribution of regional gray matter and nodal degree in  
170 explaining AC after controlling for the regional differences of AC. In a second model which is defined  
171 as AC/MC  $\sim$  TIV+ Regions \* Nodal degree + Regions \* rGM + (1| participants) we investigate the  
172 contribution of regional differences of regional gray matter and regional differences of nodal degree  
173 onto AC.

174 On the models, the volume of the entire brain (TIV) was added as a covariate because of the evidence  
175 that it is related to properties of the GM (Lüders et al., 2002). In these models all the variables are  
176 centered around zero within each subject and normalized using z-transformation. Furthermore, we  
177 statistically tested different models explaining the same outcome measure using the lme4 package in  
178 R (Bates et al., 2014).

### 179 **3.3.2 Null models**

180 To further test our hypothesis, similar to (Lee, Rodrigue, Glahn, Bassett, & Frangou, 2020), we built  
181 random null models by randomizing the structural connectivity matrix (i.e. A in equation 1) and  
182 estimated the interrelation between controllability, gray matter, degree distribution as explained in  
183 section 3.3.1. Specifically, preserving its degree distribution, we randomized matrix A 1000 times using  
184 the brain connectivity toolbox (Rubinov & Sporns, 2010) and compared the beta values of rGM in the  
185 randomized networks to that obtained in the original network.

186

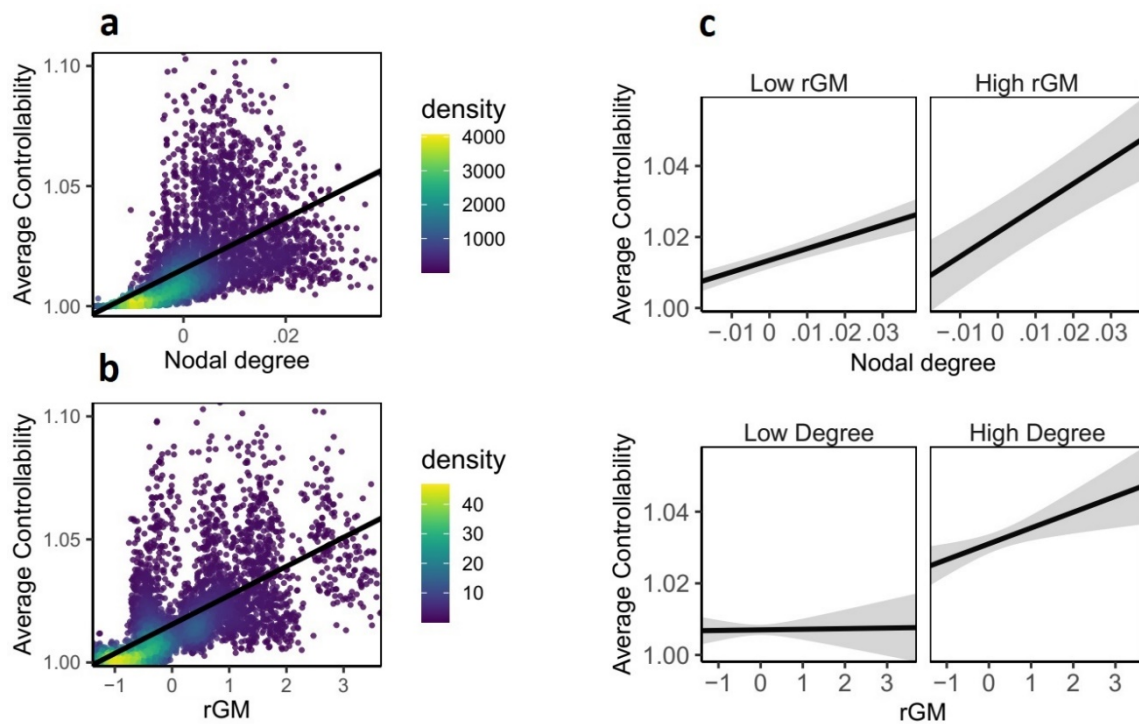
## 187 **4 Results**

### 188 **4.1 Effects of gray matter on brain controllability**

189 In a first step, we investigated if we could replicate previously reported findings that higher nodal  
190 degree relates to higher AC (see Figure 1A). We built a linear mixed effects model to predict AC based  
191 on nodal degree with subjects as a random intercept (for details see Supplementary Material-Model  
192 comparisons Table C1). Our results, summarized in Figure 1A replicates previous findings (Gu et al.,  
193 2015) suggesting that structural connectivity strength quantified in terms of nodal degree across the  
194 whole brain is positively associated with nodal AC. In the second step we investigated if, beyond this  
195 positive association between degree and AC, rGM explains additional variance of AC. To this aim, we  
196 extended our model by including regional GM volume and TIV as additional predictors to nodal degree  
197 Our results show that rGM and nodal degree are both critical to explain AC and their respective sizes  
198 of effect are comparable ( $\beta_{\text{degree}} = 0.36$  [p-value < 0.001],  $\beta_{\text{rGM}} = 0.44$  [p-value < 0.001]). Next, we



199 included regions as additional predictors to further explain AC and to improve the fitness of the model.  
 200 Our results show, that rGM and AC are significantly positively associated (see Figure 1B) and interact  
 201 with nodal degree ( $\beta=0.04$ , 95% CI:[0.01 0.07],  $p_{\text{bonf}} = 0.01$ ), suggesting that highest levels of average  
 202 controllability were best explained with concurrent high rGM and high node degree (see Figure 1C). To  
 203 verify that the AC cannot not be explained with simpler models, we compared competing models (see  
 204 Supplementary Material-Model comparisons Table C1). The results show that the full model (for  
 205 details, see the competing models Supplementary Material-Model comparisons Table C1 and the full  
 206 outcomes of the winning model in Table S1) outperformed all alternatives Finally, we used randomized  
 207 null networks (for details see section 3.3.2) to investigate if rGM would remain a significant factor. Our  
 208 results show that the contribution of rGM in the randomized networks is significantly lower than those  
 209 in the original networks ( $p$ -value < 0.001). Taken together, our results stress the interdependency  
 210 between nodal connectivity strength and GM volume for brain controllability.



211  
 212 **Figure 1:** Visualization of interaction effect of nodal degree and rGM in the mixed effects model predicting average  
 213 controllability (AC). This effect was controlled for by the TIV and regional differences of average controllability. Figure shows  
 214 that AC is best explained by WM structure and rGM together. Each dot represents one region from one subject. The density  
 215 bar shows where the majority of the data is located. (A) Association between nodal degree and AC. (B) Association between

216 rGM and AC. (C) Interaction between rGM and degree on AC suggesting that highest levels of AC are reached when both  
217 degree and rGM are high together. For visualization, median split was used to classify rGM and Degree into high and low  
218 respectively. In the original model, both effects were preserved as continuous variables.

219 Finally, in a further step, we used the same model to assess the relation between MC, rGM, and nodal  
220 degree (see Supplementary Material-Modal controllability, Figure B1). Replicating previously reported  
221 findings that MC and nodal degree relates are negatively correlated (see Supplementary Material-  
222 Modal controllability, Figure B1-a), we find that rGM explains a large part of MC variance and that the  
223 combination of nodal degree, rGM, and their interaction is necessary.

224

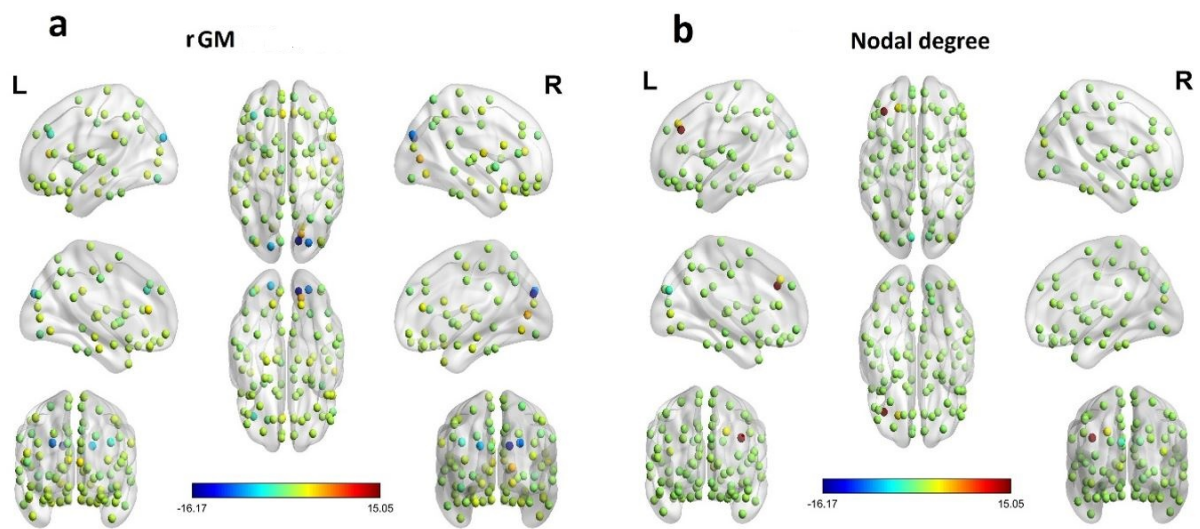
## 225 **4.2 Regional distribution of Average Controllability based on gray matter volume**

226 Further, we investigated if this global interdependency between WM and rGM (see previous section)  
227 differs on a regional level. Given our previous results that MC and AC are strongly negatively correlated  
228 and that this is reflected in the LMEs, here we focus on the AC.

229 Our results (see the competing models Supplementary Material-Model comparisons Table C2 and the  
230 full outcomes of the winning model in Table S2) show that, higher rGM and nodal degree  
231 concomitantly are associated with higher AC (see Figure 2; Table S2). Notably, highest AC levels with  
232 higher nodal degree were exhibited in the left frontal middle gyrus ( $\beta=15.11$ , 95% CI:[4.09 26.13],  $p_{\text{bonf}}$   
233 =0.007) left superior frontal gyrus ( $\beta=3.01$ , 95% CI:[.24 5.78],  $p_{\text{bonf}}=0.033$ ), which agrees with previous  
234 research also locating driver nodes for AC in the frontal lobes. Further, higher levels of AC were linked  
235 to higher levels of nodal degree in the left Calcarine ( $\beta=1.78$ , 95% CI:[.69 2.86],  $p_{\text{bonf}}=0.001$ ). There were  
236 also regions where higher levels of nodal degree exacerbated AC, with strongest effects located in the  
237 right and left cuneus (right cuneus:  $\beta=-1.34$ , 95% CI:[-2.11 -0.57],  $p_{\text{bonf}}=0.001$ ; left cuneus:  $\beta=-2.70$ , 95%  
238 CI:[-3.33 -2.08],  $p_{\text{bonf}}<0.001$ ). When turning to the relation of rGM and AC, higher rGM associated with  
239 higher AC levels in the right Calcarine ( $\beta=5.61$ , 95% CI:[4.50 6.73],  $p_{\text{bonf}}<0.001$ ), right lingual area  
240 ( $\beta=2.98$ , 95% CI:[2.63 3.33],  $p_{\text{bonf}}<0.001$ ) and the left and right anterior cingulate (left anterior

241 cingulate:  $\beta= 3.76$ , 95% CI:[2.61 4.91], $p_{\text{bonf}}<0.001$ ; right anterior cingulate:  $\beta= 2.88$ , 95% CI:[2.28  
242 3.48], $p_{\text{bonf}}<0.001$ ).

243 There were several regions exhibiting lower AC levels with higher rGM. Strongest effects were found  
244 in the right cuneus ( $\beta=-16.17$ , 95% CI:[-18.46 -13.88], $p_{\text{bonf}}<0.001$ ) and the left frontal middle gyrus ( $\beta=-$   
245 3.34, 95% CI:[-6.62 -0.07], $p_{\text{bonf}}= 0.045$ ). The finding suggests that, although on a whole brain level nodal  
246 degree and rGM are concomitantly associated with increased AC, for some regions, most notably the  
247 left frontal middle gyrus, higher nodal degree and lower rGM together exhibit higher AC (see Table S2).

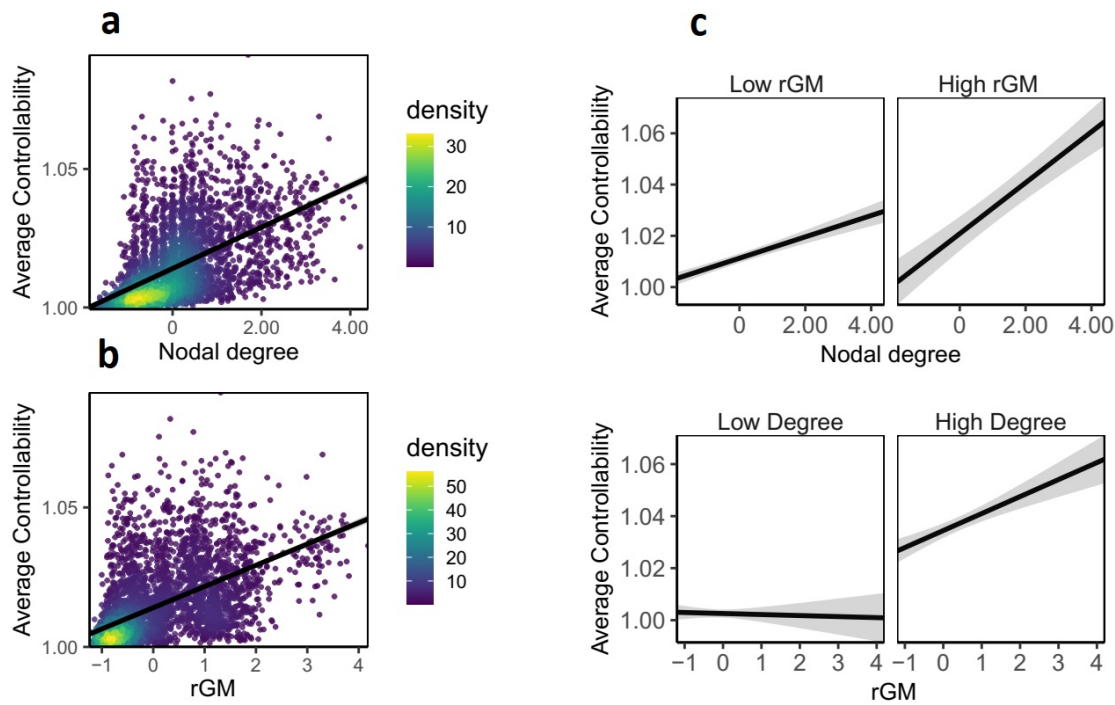


248  
249 **Figure 2:** Visualization of interaction effects of mixed effects model predicting average controllability (AC) based on regional  
250 GM (A) and regional nodal degree (B). For visualization, colors represent standardized Beta coefficients for effects of rGM  
251 and nodal degree respectively for each brain region. Higher values indicate a beneficial and lower values indicate an impeding  
252 effect of rGM /nodal degree onto AC.

### 253 4.3 Replication study

254 To investigate if the results in section 3.1. (complementary effects of rGM and nodal degree and AC  
255 and MC) are replicable, we used data from a cohort of 48 subjects from another publicly available  
256 dataset where we also used a slightly different preprocessing pipeline (see Supplementary Material-  
257 Replication study methods for details). Also, in this data set nodal degree and rGM increased AC (see  
258 Figure 3; for details see Table S3), while highest AC levels were achieved when both nodal degree and  
259 higher rGM were high together ( $\beta=0.08$ , 95% CI:[0.04 0.12],  $p_{\text{bonf}}=0.01$ ). Furthermore, rGM and nodal

260 degree both decrease MC and the lowest values of MC were achieved only for the lowest levels of rGM  
 261 and nodal degree (Supplementary Material - Modal controllability, Figure B2). Taken together, these  
 262 results suggest that this association between rGM and nodal degree is robust and not driven by  
 263 individual differences in different data sets.



264  
 265 **Figure 3:** Replication sample. AC is estimated based on WM structure but strongly relates to rGM. Each dot represents data  
 266 from one region of one subject and density bar shows where the majority of data is located. (A) Effect of nodal degree on AC.  
 267 (B) Effect of rGM on AC. (C) Interaction effect between rGM and nodal degree suggests that highest levels of AC are reached  
 268 when both degree and rGM are high together. For visualization, median split was used to classify rGM and degree into high  
 269 and low respectively. In the original model, both effects were preserved as continuous variables.

270

## 271 5 Discussion

272 In this work, we investigated how brain volumetrics contribute to global network control properties  
 273 derived from the structural connectome composed of the white matter fiber tracts. In line with (John  
 274 Dominic Medaglia et al., 2017), we hypothesized that large-scale network dynamics derived from the  
 275 structural connectome (here quantified by average and modal brain controllability) would be further

276 explained by GM structural properties. This work is, to our knowledge, the first attempt to map the  
277 interdependency of both metrics, and we discuss findings with respect to their clinical relevance.

278 We show that on average, the amount of rGM directly affects the brain's availability to dynamically  
279 transition between brain states and to adopt new modes of activity. However, levels of brain  
280 controllability were best explained when combining information from structural properties of both  
281 WM and rGM, suggesting that volumetric might provide additional information in relating brain  
282 controllability to understanding cognition, neurological and neuropsychiatric disorders, and the  
283 concept of brain reserve.

### 284 **5.1 Mediating role of GM on the relation between WM and brain controllability**

285 Our finding that nodal degree is highly predictive of brain controllability agrees with previous works  
286 (Gu et al., 2015; John D Medaglia, 2019), suggesting that the brain's ability to traverse into easy and  
287 difficult-to-reach brain states relies on strength of structural connectivity, which might reflect the  
288 degrees of freedom to steer the transition of brain states. However, our findings suggest that this  
289 picture is incomplete. Structural connectivity relies on sufficient support from GM reserves. Highest  
290 effects of AC were reached with enhanced nodal degree within frontal regions, which support the rich  
291 literature showing that frontal brain networks play a central role in initiating dynamic reconfigurations  
292 during executive cognition. However, increased rGM within that very region was negatively related to  
293 brain controllability. While within clinical populations reduced rGM is generally related to  
294 neuropathology, there is research suggesting that within healthy subjects, rGM decreases with  
295 increases of WM density throughout development from adolescence to adulthood. This finding has  
296 been related to reduced quantity of synapses resulting from synaptic pruning (Giorgio et al., 2010)  
297 which has been predominantly found in primary visual (calcarine sulcus) and prefrontal cortex (middle  
298 frontal gyrus) (Huttenlocher, 1979; Huttenlocher & Dabholkar, 1997). In our data, average brain  
299 controllability was maximal when exactly these regions showed reduced rGM and increased  
300 connectivity of the white matter connectome. One could speculate that this finding reflects more

301 efficient and developmentally advanced brain functioning in a broad range of tasks potentially related  
302 to synchronizing the actions with intentions in a goal directed way.

## 303 **5.2 Potential contribution of sensory regions to brain controllability**

304 On a functional level, we find several key visual areas to stand out with respect to both average as well  
305 as modal controllability. Enhanced rGM in the right cuneus has previously been reported to predict  
306 higher error rates in a response inhibition task in bipolar (Haldane, Cunningham, Androutsos, &  
307 Frangou, 2008) and has also been related to motor response in functional imaging studies (Booth et  
308 al., 2005; Matthews, Simmons, Arce, & Paulus, 2005). We believe that these findings suggest that the  
309 function of those primary visual areas goes far beyond unimodal information processing. Closely  
310 related, recent work suggests that primary sensory cortices might occupy more “hub-like” positions in  
311 the brain through enhanced long-distance connectivity across brain-wide communities (Esfahlani,  
312 Bertolero, Bassett, & Betzel, 2020). Taken together, we speculate that sensory regions could be ideal  
313 hot spots for brain controllability nodes. Given their high global inter-connectivity, these sensory nodes  
314 act potentially as the controllers with respect for the afferent inputs while the other regions act as  
315 controllers for efferent demands.

## 316 **5.3 Linking GM and WM in the context of controllability**

317 Cognitive functioning arises from complex re-configurations across metabolically expensive large-scale  
318 networks, facing a trade-off between wiring cost (topological efficiency) and efficient adaptation  
319 patterns between multiple neuronal populations (topological value; Bullmore & Sporns, 2012). Recent  
320 studies have suggested that the behavioral relevance of this tradeoff between topological efficiency  
321 and topological value can be described by the brain’s energy expenditure to exhibit control along large-  
322 scale structural networks. The ratio of neuronal signaling to non-signaling related metabolic energy  
323 expenditure has shown opposite directionalities for white and gray matter (Yu et al, 2018, Zhu et al  
324 2012). Here, we speculate that energy expenditure could be one of the key factors linking GM and WM  
325 in the framework of controllability analysis. AC relates to the average energy a brain region needs to

326 exert to steer the brain dynamics into all possible brain states (Gu et al., 2015; Y. N. Kenett et al., 2018;  
327 Liu, Slotine, & Barabasi, 2011) and therefore, more regional gray matter volume is more likely to  
328 provide the sufficient energy. In contrast, in absence of sufficient WM tracts i.e. lower nodal degree,  
329 rGM cannot fully force the transitions since the energy cannot be exerted. This conception has to be  
330 expressed on a behavioral level, in that the brain system's control capacity is especially sensitive to  
331 rGM. Indeed, a range of studies have suggested that rGM but not white matter changes relate to  
332 abnormal behavioral conditions, such as in antisocial personality disorder (Raine et al., 2000),  
333 medication-naive high-functioning children with autism spectrum disorder (Palmen et al., 2005), and  
334 alcohol dependent individuals (Fein et al., 2002). Closely related, MC is strongest when nodal degree  
335 and rGM are simultaneously low. MC is related to the ability to drive the brain dynamics toward  
336 difficult to reach states by change the modes of activity on the whole brain level. It is therefore  
337 conceivable to propose that similar to the relevance of nodal sparsity to enable optimal MC (Gu et al.,  
338 2015), scarcity of rGM enhances the ability of the host node by exerting more fine-grained effects that  
339 affect only a minimal set of others nodes.

#### 340 **5.4 Limitations: beyond linear full controllability**

341 Our results in the current study warrant the conclusion that the interplay of gray matter and  
342 controllability has a complex nature. Different kinds of controllability are best practiced for different  
343 values of gray matter volume. While this seems to be a satisfying first insight on the potential missing  
344 role of gray matter in studying brain controllability, there are important aspects which remain yet to  
345 be explored. The choice of nonlinear dynamics to define the range of controllability metrics could have  
346 considerable effects on our findings. For instance, it is suggested that importance of nodal geometry  
347 could actually follow opposite trends when nonlinear and control models are compared (Jiang & Lai,  
348 2019). How the nonlinearity might (re)define the role of rGM for control is an interesting question to  
349 ask. Relatedly, brain controllability metrics considered in the current paper are trajectory unspecific.  
350 This approach, although theoretically interesting and widely practiced, is of limited practical relevance.  
351 Studies of dynamical functional and structural connectivity and analysis of structural covariance have

352 reliably shown that brain state trajectories are not random, but rather follow general rules (see Gu et  
353 al., 2017; Tang & Bassett, 2018 for recent attempts to accommodate trajectory dependence within in  
354 the broader context of network control theory). Taken together, we believe that the role of GM should  
355 be further studied and possibly updated accounts of controllability introduced. An updated version can  
356 incorporate the nonlinearity of controllability indices and the rGM relevance by introducing novel  
357 metrics which are simultaneously dependent on structural connectivity and regional gray matter.

## 358 **6 Acknowledgements**

359 HJ was supported by Fortüne grant of Medical Faculty of University of Tübingen (No. 2487-1-0). AZ was  
360 supported by the Swiss National Science Foundation ([P2ZHP1\\_181435](#)). MW was supported by EU-  
361 ERA-Net: Neuromarket, EU-WIDESPREAD: Fat4BBrain, DFG Wa2673/10, and Neurobiologie  
362 motivierten Verhaltens (TPA06). The authors declare no conflict of interest.

363

## 364 **7 Author contribution statement**

365 Conceptualization: HJ, AZ, MW, SA. Methodology: HJ, SA, AM, AZ. Validation: HJ, AZ. Statistical analysis:  
366 AZ, HJ. Resources: MW, ME. Supervision: MW, ME, CG. Data Curation: VK, ML. Writing-Original Draft:  
367 AZ, HJ. Writing-Review: AZ, HJ, ME, MW, CG.

## 368 **8 Data availability statement**

369 The data used in the current study publicly available online. See Methods for detail.

## 370 **9 References**

- 371 Agosta, F., Pievani, M., Sala, S., Geroldi, C., Galluzzi, S., Frisoni, G. B., & Filippi, M. (2011). White matter  
372 damage in Alzheimer disease and its relationship to gray matter atrophy. *Radiology*, *258*(3),  
373 853-863.
- 374 Ashburner, J., & Friston, K. J. (2005). Unified segmentation. *Neuroimage*, *26*(3), 839-851.
- 375 Baayen, R. H., Davidson, D. J., & Bates, D. M. (2008). Mixed-effects modeling with crossed random  
376 effects for subjects and items. *Journal of memory and language*, *59*(4), 390-412.
- 377 Bassett, D. S., & Sporns, O. (2017). Network neuroscience. *Nature Neuroscience*, *20*(3), 353.



378 Bates, D., Maechler, M., Bolker, B., & Walker, S. (2014). lme4: Linear mixed-effects models using Eigen  
379 and S4. *R package version, 1(7)*, 1-23.

380 Bodini, B., Khaleeli, Z., Cercignani, M., Miller, D. H., Thompson, A. J., & Ciccarelli, O. (2009). Exploring  
381 the relationship between white matter and gray matter damage in early primary progressive  
382 multiple sclerosis: an in vivo study with TBSS and VBM. *Human Brain Mapping, 30(9)*, 2852-  
383 2861.

384 Boisgontier, M. P., & Cheval, B. (2016). The anova to mixed model transition. *Neuroscience &*  
385 *Biobehavioral Reviews, 68*, 1004-1005.

386 Booth, J. R., Burman, D. D., Meyer, J. R., Lei, Z., Trommer, B. L., Davenport, N. D., . . . Marsel Mesulam,  
387 M. (2005). Larger deficits in brain networks for response inhibition than for visual selective  
388 attention in attention deficit hyperactivity disorder (ADHD). *Journal of Child Psychology and*  
389 *Psychiatry, 46(1)*, 94-111.

390 Braun, U., Harneit, A., Pergola, G., Menara, T., Schaefer, A., Betzel, R. F., . . . Chen, J. (2019). Brain state  
391 stability during working memory is explained by network control theory, modulated by  
392 dopamine D1/D2 receptor function, and diminished in schizophrenia. *arXiv preprint*  
393 *arXiv:1906.09290*.

394 Bullmore, E., & Sporns, O. (2012). The economy of brain network organization. *Nature Reviews*  
395 *Neuroscience, 13(5)*, 336.

396 Douaud, G., Smith, S., Jenkinson, M., Behrens, T., Johansen-Berg, H., Vickers, J., . . . Matthews, P. M.  
397 (2007). Anatomically related grey and white matter abnormalities in adolescent-onset  
398 schizophrenia. *Brain, 130(9)*, 2375-2386.

399 Esfahlani, F. Z., Bertolero, M. A., Bassett, D. S., & Betzel, R. F. (2020). Space-independent community  
400 and hub structure of functional brain networks. *Neuroimage, 116612*.

401 Fein, G., Di Sclafani, V., Cardenas, V., Goldmann, H., Tolou-Shams, M., & Meyerhoff, D. J. (2002).  
402 Cortical gray matter loss in treatment-naive alcohol dependent individuals. *Alcoholism: Clinical*  
403 *and Experimental Research, 26(4)*, 558-564.

404 Giorgio, A., Watkins, K. E., Chadwick, M., James, S., Winmill, L., Douaud, G., . . . Johansen-Berg, H.  
405 (2010). Longitudinal changes in grey and white matter during adolescence. *Neuroimage, 49(1)*,  
406 94-103.

407 Glasser, M. F., Sotiropoulos, S. N., Wilson, J. A., Coalson, T. S., Fischl, B., Andersson, J. L., . . . Polimeni,  
408 J. R. (2013). The minimal preprocessing pipelines for the Human Connectome Project.  
409 *Neuroimage, 80*, 105-124.

410 Gu, S., Betzel, R. F., Mattar, M. G., Cieslak, M., Delio, P. R., Grafton, S. T., . . . Bassett, D. S. (2017).  
411 Optimal trajectories of brain state transitions. *Neuroimage, 148*, 305-317.  
412 doi:10.1016/j.neuroimage.2017.01.003

413 Gu, S., Pasqualetti, F., Cieslak, M., Telesford, Q. K., Yu, A. B., Kahn, A. E., . . . Bassett, D. S. (2015).  
414 Controllability of structural brain networks. *Nature Communications, 6*. doi:ARTN 8414  
415 10.1038/ncomms9414

416 Haldane, M., Cunningham, G., Androustos, C., & Frangou, S. (2008). Structural brain correlates of  
417 response inhibition in Bipolar Disorder I. *Journal of Psychopharmacology, 22(2)*, 138-143.

418 Huttenlocher, P. R. (1979). Synaptic density in human frontal cortex-developmental changes and  
419 effects of aging. *Brain Res, 163(2)*, 195-205.

420 Huttenlocher, P. R., & Dabholkar, A. S. (1997). Regional differences in synaptogenesis in human  
421 cerebral cortex. *Journal of comparative Neurology, 387(2)*, 167-178.

422 Jeganathan, J., Perry, A., Bassett, D. S., Roberts, G., Mitchell, P. B., & Breakspear, M. (2018). Fronto-  
423 limbic dysconnectivity leads to impaired brain network controllability in young people with  
424 bipolar disorder and those at high genetic risk. *NeuroImage: Clinical, 19*, 71-81.

425 Jenkinson, M., Bannister, P., Brady, M., & Smith, S. (2002). Improved optimization for the robust and  
426 accurate linear registration and motion correction of brain images. *Neuroimage, 17(2)*, 825-  
427 841.

428 Jenkinson, M., & Smith, S. (2001). A global optimisation method for robust affine registration of brain  
429 images. *Medical image analysis, 5(2)*, 143-156.

430 Jeurissen, B., Tournier, J.-D., Dhollander, T., Connelly, A., & Sijbers, J. (2014). Multi-tissue constrained  
431 spherical deconvolution for improved analysis of multi-shell diffusion MRI data. *Neuroimage*,  
432 *103*, 411-426.

433 Jiang, J., & Lai, Y.-C. (2019). Irrelevance of linear controllability to nonlinear dynamical networks.  
434 *Nature Communications*, *10*(1), 1-10.

435 Kailath, T. (1980). *Linear systems* (Vol. 156): Prentice-Hall Englewood Cliffs, NJ.

436 Kalman, R. E. (1963). Mathematical description of linear dynamical systems. *Journal of the Society for*  
437 *Industrial and Applied Mathematics, Series A: Control*, *1*(2), 152-192.

438 Kenett, Y. N., Beaty, R. E., & Medaglia, J. D. (2018). A computational network control theory analysis of  
439 depression symptoms. *Personality neuroscience*, *1*.

440 Kenett, Y. N., Medaglia, J. D., Beaty, R. E., Chen, Q., Betzel, R. F., Thompson-Schill, S. L., & Qiu, J. (2018).  
441 Driving the brain towards creativity and intelligence: A network control theory analysis.  
442 *Neuropsychologia*. doi:10.1016/j.neuropsychologia.2018.01.001

443 Kong, L., Herold, C. J., Zöllner, F., Salat, D. H., Lässer, M. M., Schmid, L. A., . . . Schad, L. R. (2015).  
444 Comparison of grey matter volume and thickness for analysing cortical changes in chronic  
445 schizophrenia: a matter of surface area, grey/white matter intensity contrast, and curvature.  
446 *Psychiatry Research: Neuroimaging*, *231*(2), 176-183.

447 Lee, W. H., Rodrigue, A., Glahn, D. C., Bassett, D. S., & Frangou, S. (2020). Heritability and cognitive  
448 relevance of structural brain controllability. *Cereb Cortex*, *30*(5), 3044-3054.

449 Liu, Y. Y., Slotine, J. J., & Barabasi, A. L. (2011). Controllability of complex networks. *Nature*, *473*(7346),  
450 167-173. doi:10.1038/nature10011

451 Lüders, E., Steinmetz, H., & Jäncke, L. (2002). Brain size and grey matter volume in the healthy human  
452 brain. *Neuroreport*, *13*(17), 2371-2374.

453 Matthews, S. C., Simmons, A. N., Arce, E., & Paulus, M. P. (2005). Dissociation of inhibition from error  
454 processing using a parametric inhibitory task during functional magnetic resonance imaging.  
455 *Neuroreport*, *16*(7), 755-760.

456 Medaglia, J. D. (2019). Clarifying cognitive control and the controllable connectome. *Wiley*  
457 *Interdisciplinary Reviews: Cognitive Science*, *10*(1), e1471.

458 Medaglia, J. D., Pasqualetti, F., Hamilton, R. H., Thompson-Schill, S. L., & Bassett, D. S. (2017). Brain and  
459 cognitive reserve: translation via network control theory. *Neuroscience & Biobehavioral*  
460 *Reviews*, *75*, 53-64.

461 Medaglia, J. D., Zurn, P., Sinnott-Armstrong, W., & Bassett, D. S. (2017). Mind control as a guide for the  
462 mind. *Nature Human Behaviour*, *1*(6). doi:UNSP 0119

463 10.1038/s41562-017-0119

464 Muldoon, S. F., Pasqualetti, F., Gu, S., Cieslak, M., Grafton, S. T., Vettel, J. M., & Bassett, D. S. (2016).  
465 Stimulation-based control of dynamic brain networks. *PLoS computational biology*, *12*(9),  
466 e1005076.

467 Palmén, S. J., Pol, H. E. H., Kemner, C., Schnack, H. G., Durston, S., Lahuis, B. E., . . . Van Engeland, H.  
468 (2005). Increased gray-matter volume in medication-naïve high-functioning children with  
469 autism spectrum disorder. *Psychological Medicine*, *35*(4), 561-570.

470 Pasqualetti, F., Zampieri, S., & Bullo, F. (2014). Controllability metrics, limitations and algorithms for  
471 complex networks. *IEEE Transactions on Control of Network Systems*, *1*(1), 40-52.

472 Raine, A., Lencz, T., Bihrlé, S., LaCasse, L., & Colletti, P. (2000). Reduced prefrontal gray matter volume  
473 and reduced autonomic activity in antisocial personality disorder. *Archives of General*  
474 *Psychiatry*, *57*(2), 119-127.

475 Rubinov, M., & Sporns, O. (2010). Complex network measures of brain connectivity: uses and  
476 interpretations. *Neuroimage*, *52*(3), 1059-1069.

477 Tang, E., & Bassett, D. S. (2018). Colloquium: Control of dynamics in brain networks. *Reviews of Modern*  
478 *Physics*, *90*(3), 031003.

479 Tournier, J. D., Calamante, F., & Connelly, A. (2012). MRtrix: diffusion tractography in crossing fiber  
480 regions. *International journal of imaging systems and technology*, *22*(1), 53-66.

481 Tzourio-Mazoyer, N., Landeau, B., Papathanassiou, D., Crivello, F., Etard, O., Delcroix, N., . . . Joliot, M.  
482 (2002). Automated anatomical labeling of activations in SPM using a macroscopic anatomical  
483 parcellation of the MNI MRI single-subject brain. *Neuroimage*, *15*(1), 273-289.

484 Van Essen, D. C., Ugurbil, K., Auerbach, E., Barch, D., Behrens, T., Bucholz, R., . . . Curtiss, S. W. (2012).  
485 The Human Connectome Project: a data acquisition perspective. *Neuroimage*, *62*(4), 2222-  
486 2231.

487 Villain, N., Desgranges, B., Viader, F., De La Sayette, V., Mézenge, F., Landeau, B., . . . Chételat, G.  
488 (2008). Relationships between hippocampal atrophy, white matter disruption, and gray matter  
489 hypometabolism in Alzheimer's disease. *Journal of Neuroscience*, *28*(24), 6174-6181.

490 Winkler, A. M., Kochunov, P., Blangero, J., Almasy, L., Zilles, K., Fox, P. T., . . . Glahn, D. C. (2010). Cortical  
491 thickness or grey matter volume? The importance of selecting the phenotype for imaging  
492 genetics studies. *Neuroimage*, *53*(3), 1135-1146.

493 Zhu, X.-H., Qiao, H., Du, F., Xiong, Q., Liu, X., Zhang, X., . . . Chen, W. (2012). Quantitative imaging of  
494 energy expenditure in human brain. *Neuroimage*, *60*(4), 2107-2117.

495 Zoeller, D., Sandini, C., Schaer, M., Eliez, S., Bassett, D., & Van De Ville, D. (2019). Structural control  
496 energy of resting-state functional brain states reveals inefficient brain dynamics in psychosis  
497 vulnerability. *bioRxiv*, 703561.

498